Inorganic Chemistry

Article

pubs.acs.org/IC

Turning on Red and Near-Infrared Phosphorescence in Octahedral Complexes with Metalated Quinones

Aurélie Damas,[†] Barbara Ventura,[‡] Jamal Moussa,[†] Alessandra Degli Esposti,[‡] Lise-Marie Chamoreau,[†] Andrea Barbieri,*[,†,‡] and Hani Amouri*[,†]

[†]Institut Parisien de Chimie Moléculaire, UMR 7201, Université Pierre et Marie Curie, Paris 6, 4 place Jussieu, case 42, 75252 Paris Cedex 05, France

[‡]Istituto per la Sintesi Organica e la Fotoreattività (ISOF), Consiglio Nazionale delle Ricerche (CNR), Via Gobetti 101, 40129 Bologna, Italy

Supporting Information

ABSTRACT: We report the synthesis of π-bonded ruthenium, rhodium, and iridium *o*-benzoquinones $[Cp^*M(o\text{-}C_6H_4O_2)]^n$ [M = Ru (**2**), n = 1−; Rh (**3**), n = 0; Ir (**4**), n = 0] following a novel synthetic procedure. Compounds **2**−**4** were fully characterized by spectroscopic methods and used as chelating *organometallic linkers*, "OM-linkers", toward luminophore bricks such as $Ru(bpy)_2^{2+}$, $Rh(ppy)_2^{+}$, and $Ir(ppy)_2^{+}$ (bpy = 2,2′-bipyridine; ppy = 2-phenylpyridine) for the design of a novel family of octahedral bimetallic complexes of the general formula $[(L\text{-}L)_2M(OM\text{-}linkers)][X]_m$ (X = counteranion; m = 0, 1, 2) whose luminescent properties depend on the choice of the OM-linker and the luminophore brick. Thus, dinuclear assemblies such as $[(bpy)_2Ru(2)][OTf]$ (**5**-OTf), $[(bpy)_2Ru(2)][\Delta\text{-TRISPHAT}]$ (**5**-ΔT) {TRISPHAT = tris[tetrachlorobenzene-1,2-bis(olato)]phosphate}, $[(bpy)_2Ru(3)][OTf]_2$ (**6**-OTf), $[(bpy)_2Ru(4)][OTf]_2$ (**7**-OTf), $[(bpy)_2Ru(4)][\Delta\text{-TRISPHAT}]_2$ (**7**-ΔT), $[(ppy)_2Rh(2)]$ (**8**), $[(ppy)_2Rh(3)][OTf]$ (**9**-OTf), $[(ppy)_2Rh(4)][OTf]$ (**10**-OTf), $[(ppy)_2Rh(4)][\Delta\text{-TRISPHAT}]$ (**10**-ΔT), $[(ppy)_2Ir(2)]$ (**11**), $[(ppy)_2Ir(3)][OTf]$ (**12**-OTf), $[(ppy)_2Ir(4)][OTf]$ (**13**-OTf), and $[(ppy)_2Ir(4)][\Delta\text{-TRISPHAT}]$ (**13**-ΔT) were prepared and fully characterized. The X-ray molecular structures of three of them, i.e., **5**-OTf, **8**, and **11**, were determined. The structures displayed a main feature: for instance, the two oxygen centers of the OM-linker $[Cp^*Ru(o\text{-}C_6H_4O_2)]^-$ (**2**) chelate the octahedral chromophore metal center, whether it be ruthenium, rhodium, or iridium. Further, the carbocycle of the OM-linker **2** adopts a η^4-quinone form but with some catecholate contribution due to metal coordination. All of these binuclear assemblies showed a wide absorption window that tailed into the near-IR (NIR) region, in particular in the case of the binuclear ruthenium complex **5**-OTf with the anionic OM-linker **2**. The latter feature is no doubt related to the effect of the OM-linker, which lights up the luminescence in these homo- and heterobinuclear compounds, while no effect has been observed on the UV−visible and emission properties because of the counteranion, whether it be triflate (OTf) or Δ-TRISPHAT. At low temperature, all of these compounds become luminescent; remarkably, the *o*-quinonoid linkers $[Cp^*M(o\text{-}C_6H_4O_2)]^n$ (**2**−**4**) turn on red and NIR phosphorescence in the binuclear octahedral species **5**−**7**. This trend was even more observable when the ruthenium OM-linker **2** was employed. These assemblies hold promise as NIR luminescent materials, in contrast to those made from organic 1,2-dioxolene ligands that conversely are not emissive.

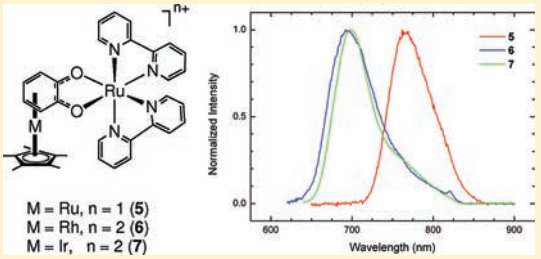

INTRODUCTION

Coordination chemistry of transition-metal complexes of the redox-active 1,2-dioxolene chelating ligands, and their structural analogues with other donor atoms, has been extensively studied since the mid 1970s by the group of Hendrickson and Pierpont,[1] and later by the groups of Lever[2] and Ward and McCleverty,[3] because of their intriguing electronic properties.[4] These bidentate ligands show three oxidation states {[catecholate]$^{2-}$ (cat^{2-}), [semiquinone]$^-$ (sq^-), and quinone (q)} related to one-electron transformations, which in combination with redox-active metal atoms provide complexes with rich electrochemical and spectroscopic behavior.[5] In these complexes, a strong degree of orbital mixing between metal d(π) and ligand p(π) frontier orbitals renders conventional assignment of the oxidation state, based on localized charges, difficult.[2] The different redox states of dioxolene ligands generally have distinct spectroscopic characteristics, and their metal complexes show intense charge-transfer (CT) bands appearing in different regions of the spectrum as the oxidation state changes.[4a] For instance, ruthenium complexes show a strong near-IR (NIR) absorption when the ligand is in the semiquinone form $[Ru^{II}/sq^-]$, due to a Ru(dπ) → sq(π^*) metal-to-ligand CT (MLCT) band that disappears in the fully reduced catecholate form $[Ru^{II}/cat^{2-}]$ or is moved to higher energy in the visible region in the oxidized $[Ru^{II}/q]$ state.[3]

A number of applications have been described, stemming from fundamental studies on noninnocent ligands and their

Received: September 20, 2011
Published: January 19, 2012

   dx.doi.org/10.1021/ic202021w | Inorg. Chem. 2012, 51, 1739−1750

Chart 1. OM-Linkers 2−4 and the Related Luminescent Assemblies 5−13

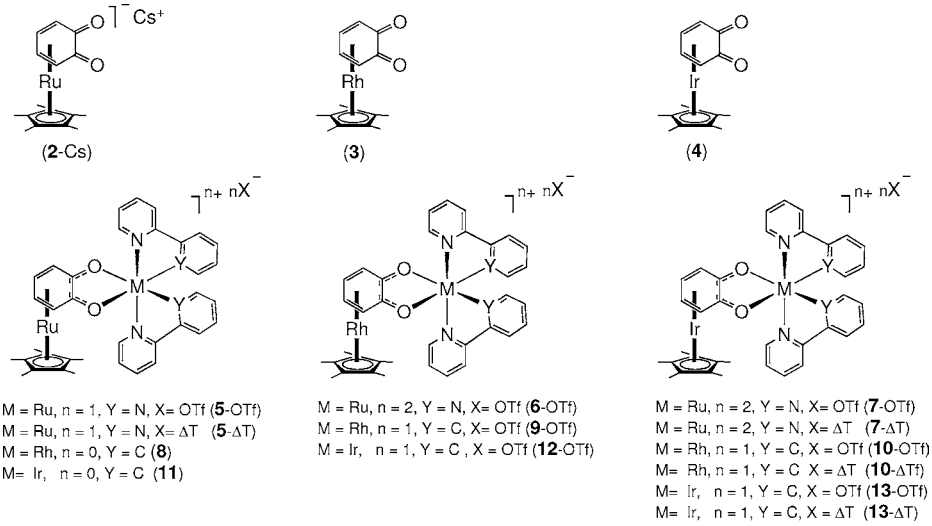

metal complexes; e.g., they have been proposed as redox-switchable electrochromic dyes, for modulation of optical signals and smart windows,[6] as magnetic materials,[7] as NIR sensitizers[8] and anchors[9] to semiconductor surfaces in organic photovoltaic cells and in applications related to solar energy conversion,[4b] as components of modified electrodes,[10] and as extended assemblies for electron and energy transfer incorporating both organic and coordination compounds.[11] Although the spectroelectrochemical richness of this series of metal dioxolene complexes has generated a number of fundamental studies and technological applications, at the same time it has prevented, until now, the observation of their luminescence properties, which may pave the way to a number of new applications. In fact, the redox-active substituents introduce accessible low-energy electronic transitions, which lead to quenching of the metal center luminescence by an electron-transfer mechanism.

The research in this area has been focused mainly on d^6 transition-metal complexes,[12] such as ruthenium,[3,13] osmium,[14] chromium,[15] manganese,[16] and rhenium,[17] and on the properties of the electronic ground states of such compounds, while there have been fewer reports on the properties of rhodium,[18] iridium,[19] and platinum[20] complexes with dioxolene ligands.

We previously reported the synthesis of organometallic (OM) benzoquinone complexes $[Cp^*M(o\text{-}C_6H_4O_2)]$ (M = Rh, Ir; Cp* = pentamethylcyclopentadienyl)[21] and, more recently, the related thio-[22] and selenoquinone metal complexes.[23] These metalated quinonoid compounds were found to be adequate OM-linkers for the preparation of unique types of supramolecular assemblies[18a,21c,24] with useful luminescent properties.[25] More recently, we discovered that the use of different metals in the OM-linker allowed us to optimize the electronic properties of an octahedral $[Ru(bpy)_2(o\text{-}C_6H_4O_2)]^{2+}$ complex, giving rise to materials with panchromatic absorption with high oscillator strengths and unprecedented luminescent behavior.[26] Because this complex-as-ligand approach proved to be very effective in the modulation of the electronic properties of ruthenium(II) polypyridyl complexes, it turned out to also be useful for the preparation of a novel class of complexes with metalated dioxolene ligands. In this paper, we report on the synthesis and photophysical characterization of a series of bimetallic ruthenium polypyridine and rhodium and iridium cyclometalated complexes (Chart 1) showing strong luminescence in condensed media. Here π-bonded ruthenium, rhodium, and iridium *o*-benzoquinone complexes act as chelating units for the $[Ru(bpy)_2]^{2+}$ or $[M(ppy)_2]^{+}$ moieties (M = Rh, Ir). The properties of the relevant monometallic sandwich complexes $[Cp^*M(o\text{-}C_6H_4O_2)]^n$ (M = Ru, n = 1−; M = Rh, Ir, n = 0) have also been reported for comparison purposes, thus presenting the results of the studies on a series of nine bimetallic and three monometallic complexes. Using density functional theory (DFT) and time-dependent DFT (TD-DFT) methods, we derived a range of physical properties that can be tied to experimental data to help to elucidate the origin of the peculiar electronic behavior of this class of complexes.

EXPERIMENTAL SECTION

General Experimental Methods. ^{1}H NMR spectra were recorded at 300 MHz in CD_2Cl_2, and data are reported as follows: chemical shift in ppm from tetramethylsilane (TMS) with the solvent as an internal indicator (CD_2Cl_2, δ 5.33 ppm), multiplicity (s = singlet, d = doublet, t = triplet, q = quartet, m = multiplet, or overlap of nonequivalent resonances), and integration. ^{13}C NMR spectra were recorded at 75.4 MHz in CD_2Cl_2, and data are reported as follows: chemical shift in ppm from TMS with the solvent as an internal indicator (CD_2Cl_2, δ 53.84 ppm) and multiplicity with respect to proton (deduced from DEPT experiments). Glassware was oven-dried prior to use. All reactions were carried out under an argon atmosphere. Tetrahydrofuran (THF) and diethyl ether were distilled from sodium−benzophenone. CH_2Cl_2 was distilled from CaH_2. Other reagents were obtained from commercial suppliers and used as received. IR spectra were measured using a Tensor 27 (ATR diamond) Bruker spectrometer. IR data are reported as characteristic bands (cm^{-1}). The syntheses of the binuclear complexes $[(bpy)_2Ru(\mathbf{3})][OTf]_2$ (**6**-OTf), $[(bpy)_2Ru(\mathbf{4})][OTf]_2$ (**7**-OTf), $[(ppy)_2Rh(\mathbf{3})][OTf]$ (**9**-OTf), $[(ppy)_2Rh(\mathbf{4})][OTf]$ (**10**-OTf), $[(ppy)_2Ir(\mathbf{3})][OTf]$ (**12**-OTf), and $[(ppy)_2Ir(\mathbf{4})][OTf]$ (**13**-OTf) were carried out according to published procedures.[18a] Elemental analyses were performed by microanalytical services of ICSN at Gif-sur-Yvette on a Perkin-Elmer 2400 apparatus.

Synthesis of [Cp*Ru(η^6-catechol)][OTf] (1). A Schlenk flask under argon was charged with $[Cp^*Ru(CH_3CN)_3][OTf]$[27] (275 mg, 0.54 mmol) and CH_2Cl_2 (10 mL) at room temperature. Once dissolved, 1 equiv of 1,2-dihydroxybenzene (60 mg, 0.54 mmol) was added to the solution. The reaction was stirred overnight at room

dx.doi.org/10.1021/ic202021w | Inorg. Chem. 2012, 51, 1739−1750

temperature. After that, the reaction was evaporated to dryness. The brown solid was crystallized from CH_2Cl_2/Et_2O to afford an off-white solid (232 mg, 86% yield). ^1H NMR (300 MHz, CD_2Cl_2): δ 7.99 (br s, 2H, OH), 5.80 (m, 2H, π-arene), 5.21 (m, 2H, π-arene), 1.90 (s, 15H, Cp*). ^{13}C NMR (74.5 MHz, CD_2Cl_2): δ 120.4 (C−OH π-arene), 95.7 (C═C Cp*), 82.7 (C−H π-arene), 77.0 (C−H π-arene), 10.5 (CH_3 Cp*). IR (ATR, cm^{-1}): 2921, 1548, 1480, 1435, 1384, 1354, 1293, 1216, 1156, 1073, 1014, 858, 760, 670, 632, 568, 515, 462, 400, 382, 359, 307, 249, 234. Anal. Calcd for $C_{17}H_{21}F_3O_5RuS$ (495.48 g·mol^{-1}): C, 41.21; H, 4.27. Found: C, 41.02; H, 4.24.

Synthesis of [Cs][Cp*Ru(η^4-$C_6H_4O_2$)] (2-Cs). A Schlenk flask under argon was charged with Cs_2CO_3 (65.2 mg, 0.2 mmol) in CH_2Cl_2 (5 mL). To this white suspension was added a light-yellow solution of **1** (50.0 mg, 0.1 mmol) in CH_2Cl_2 (5 mL) kept under argon. The reaction mixture turned immediately to clear yellow and was stirred for 16 h, during which a gray precipitate was formed with a yellow supernatant solution. The mixture was kept at low temperature and then filtered, and the supernatant CH_2Cl_2 phase was separated. Subsequent evaporation under vacuum provided an off-white microcrystalline solid identified as [Cs][Cp*Ru(η^4-*o*-$C_6H_4O_2$)] (31.8 mg, 0.07 mmol). Yield: 70%. ^1H NMR (300 MHz, CD_2Cl_2): δ 5.07 (m, 2H, diene), 4.74 (m, 2H, diene), 1.80 (s, 15H, Cp*). ^{13}C NMR (75.4 MHz, CD_2Cl_2): δ 131.5 (C═O diene), 91.5 (C═C Cp*), 79.4 (C−H diene), 76.0 (C−H diene), 10.9 (CH_3 Cp*). IR (ATR, cm^{-1}): 3659, 3051, 2963, 2901, 1664, 1537, 1483, 1431, 1382, 1336, 1258, 1240, 1183, 1069, 1008, 876, 790, 752, 681, 637, 582, 520, 485, 457, 395, 352, 308, 240, 206. This compound was moisture-sensitive, and hence no microanalytical data were obtained.

Synthesis of [(bpy)$_2$RuCp*Ru(η^4-$C_6H_4O_2$)][OTf] (5-OTf). A Schlenk flask under argon was charged with [(bpy)$_2$RuCl$_2$] (97.8 mg, 0.2 mmol) and dissolved in acetone (10 mL). Once dissolved, 2 equiv of AgOTf (103.7 mg, 0.4 mmol) was added to the dark-purple solution. After 20 min, a white precipitate formed (AgCl) and the solution turned purple. The reaction was stirred at room temperature for 1 h. Meanwhile, in another Schlenk flask kept under argon, **1** (100 mg, 0.20 mmol) was dissolved in acetone (10 mL) and 2 equiv of Cs_2CO_3 (131.5 mg, 0.40 mmol) was added at once. The reaction was stirred for 1 h. The filtered purple solution of $[(bpy)_2Ru]^{2+}$ was added to the catecholate ruthenium complex suspension and stirred for an additional 1 h. Then the solvent was removed under vacuum, and the residue was dissolved in CH_2Cl_2 and filtered through alumina. Evaporation of CH_2Cl_2 under vacuum provided the bimetallic complex as a dark-purple microcrystalline solid (167 mg, 91% yield). ^1H NMR (300 MHz, CD_2Cl_2): δ 9.33 (1H, d, J = 5.5 Hz, H bpy), 8.99 (1H, d, J = 5.0 Hz, H bpy), 8.39 (1H, d, J = 8.3 Hz, H bpy), 8.25 (2H, m, H bpy), 8.09 (1H, d, J = 8.1 Hz, H bpy), 8.07 (dt, 1H, J = 1.5 and 7.9 Hz, H bpy), 7.90 (dt, 1H, J = 1.4 and 7.9 Hz, H bpy), 7.77 (m, 1H, H bpy), 7.67 (m, 2H, H bpy), 7.59 (dt, 1H, J = 1.4 and 8.2 Hz, H bpy), 7.47 (ddd, 1H, J = 1.3, 5.8, and 7.2 Hz, H bpy), 7.38 (d, 1H, J = 5.8 Hz, H bpy), 7.05 (ddd, 1H, J = 1.3, 5.9, and 7.2 Hz, H bpy), 6.98 (ddd, 1H, J = 1.4, 5.8, and 7.3 Hz, H bpy), 4.99 (dd, 1H, J = 1.2 and 5.3 Hz, H π-arene), 4.83 (dd, 1H, J = 1.2 and 5.4 Hz, H π-arene), 4.45 (m, 2H, H π-arene), 1.64 (s, 15H, Cp*). ^{13}C NMR (75.4 MHz, CD_2Cl_2): δ 160.7 (C═O π-arene), 158.8 (C═C bpy), 158.5 (C═C bpy), 153.7 (C−H bpy), 152.9 (C−H bpy), 152.4 (C−H bpy), 151.3 (C−H bpy), 148.8 (C═C bpy), 143.3 (C═C bpy), 135.4 (C−H bpy), 134.3 (C−H bpy), 133.5 (C−H bpy), 126.9 (C−H bpy), 126.1 (C−H bpy), 125.9 (C−H bpy), 125.4 (C−H bpy), 123.7 (C−H bpy), 123.6 (C−H bpy), 123.5 (C−H bpy), 123.2 (C−H bpy), 90.4 (Cq Cp*), 78.5 (C−H π-arene), 77.5 (C−H π-arene), 77.2 (C−H π-arene), 76.0 (C−H π-arene), 11.094 (CH_3 Cp*). IR (ATR, cm^{-1}): 3460, 3067, 2963, 2908, 1694, 1600, 1462, 1418, 1382, 1351, 1253, 1147, 1028, 1013, 866, 848, 818, 801, 762, 727, 656, 634, 603, 571, 539, 531, 515, 485, 425, 381, 341, 328, 308. Anal. Calcd for $C_{37}H_{35}F_3N_4O_5Ru_2S$ (906.90 g·mol^{-1}): C, 49.00; H, 3.89. Found: C, 49.23; H, 4.09.

Synthesis of [(bpy)$_2$RuCp*Ru(η^4-$C_6H_4O_2$)][Δ-TRISPHAT] (5-ΔT). The bimetallic ruthenium complex **5**-OTf (80 mg, 0.09 mmol) was dissolved in CH_2Cl_2 (8 mL). Then 1 equiv of [cinchonidinium]-[Δ-TRISPHAT] (94 mg, 0.09 mmol) was added to the solution. After 1 h of reaction, the solution was evaporated to dryness and the dark-purple solid was passed through a flash chromatography column (alumina/CH_2Cl_2). The Δ-TRISPHAT complex was obtained as a dark-purple microcrystalline solid and recrystallized from CH_3CN/Et_2O (94 mg, 70% yield). ^1H NMR (300 MHz, CD_2Cl_2): δ 9.32 (m, 1H, H bpy), 8.98 (d, 1H, J = 5.4 Hz, H bpy), 8.32 (dd, 1H, J = 5.6 and 7.7 Hz, H bpy), 8.18 (m, 2H, H bpy), 8.09 (d, 1H, J = 8.1 Hz, H bpy), 8.01 (q, 1H, J = 7.4 Hz, H bpy), 7.84 (m, 1H, m, H bpy), 7.75 (m, 1H, H bpy), 7.65 (m, 2H, H bpy), 7.54 (m, 1H, H bpy), 7.45 (t, 1H, J = 6.4 Hz, H bpy), 7.38 (d, 1H, J = 4.6 Hz, H bpy), 7.03 (m, 1H, H bpy), 6.98 (m, 1H, H bpy), 4.98 (d, 1H, J = 5.2 Hz, H π-arene), 4.83 (dd, 1H, J = 1.1 and 5.4 Hz, H π-arene), 4.45 (m, 2H, H π-arene), 1.65 (s, 15H, CH_3 Cp *). IR (ATR, cm^{-1}): 2921, 1695, 1596, 1446, 1387, 1351, 1290, 1256, 1235, 1009, 989, 820, 758, 717, 669, 619, 603, 583, 564, 551, 488, 455, 405, 370, 342, 329. Anal. Calcd for $C_{54}H_{35}Cl_{12}N_4O_8PRu_2{\cdot}2CH_3CN$ (1608.53 g·mol^{-1}): C, 43.31; H, 2.57. Found: C, 43.31; H, 2.80.

Synthesis of [(ppy)$_2$RhCp*Ru(η^4-$C_6H_4O_2$)] (8). A Schlenk flask was charged under argon with $[(ppy)_2Rh(\mu\text{-}Cl)]_2$ (45.1 mg, 0.05 mmol) and dissolved in acetone (5 mL). Once dissolved, 2 equiv of AgOTf (25.9 mg, 0.1 mmol) was added to the green solution. After 20 min, a white precipitate formed (AgCl) and the solution turned yellow. The reaction was stirred at room temperature for 1 h. Meanwhile, in another Schlenk flask, **1** (50 mg, 0.10 mmol) was dissolved in acetone (5 mL) and 2 equiv of Cs_2CO_3 (65.8 mg, 0.20 mmol) was added at once. The reaction was stirred for 1 h to form in situ [Cs][Cp*Ru-(catecholate)]. The filtered yellow solution of $[(ppy)_2Rh(solvent)_2]^+$ was added to the [Cs][Cp*Ru(catecholate)] suspension and stirred for an additional 1 h. Then the solvent was removed under vacuum, and the residue was dissolved in CH_2Cl_2 and filtered through Celite. Evaporation of CH_2Cl_2 under vacuum provided the bimetallic complex as a light-green solid (58 mg, 76% yield). ^1H NMR (300 MHz, CD_2Cl_2): δ 9.11 (d, 1H, J = 5.8 Hz, H ppy), 8.69 (d, 1H, J = 5.7 Hz, H ppy), 7.90 (m, 2H, H ppy), 7.78 (m, 2H, H ppy), 7.64 (d, 1H, J = 7.6 Hz, H ppy), 7.57 (d, 1H, J = 7.9 Hz, H ppy), 7.37 (dt, 1H, J = 2.7 and 5.7 Hz, H ppy), 7.12 (m, 1H, H ppy), 6.88 (m, 2H, H ppy), 6.74 (m, 2H, H ppy), 6.20 (d, 1H, J = 7.7 Hz, H ppy), 6.05 (d, 1H, J = 7.7 Hz, H ppy), 4.91 (d, 1H, J = 5.5 Hz, H π-arene), 4.82 (d, 1H, J = 5.5 Hz, H π-arene), 4.42 (m, 2H, H π-arene), 1.71 (s, 15H, CH_3 Cp*). IR (ATR, cm^{-1}): 3041, 2966, 2905, 1645, 1602, 1578, 1564, 1467, 1412, 1380, 1336, 1299, 1266, 1226, 1156, 1060, 1025, 866, 838, 793, 753, 729, 667, 649, 628, 612, 592, 528, 459, 416, 373, 349, 326. Anal. Calcd for $C_{38}H_{35}N_2O_2RhRu{\cdot}H_2O$ (773.69 g·mol^{-1}): C, 58.99; H, 4.82. Found: C, 59.20; H, 4.93.

Synthesis of [(ppy)$_2$IrCp*Ru(η^4-$C_6H_4O_2$)] (11). A Schlenk flask was charged under argon with $[(ppy)_2Ir(\mu\text{-}Cl)]_2$ (54.0 mg, 0.05 mmol) and dissolved in acetone (5 mL). Once dissolved, 2 equiv of AgOTf (25.9 mg, 0.1 mmol) was added to the yellow solution. After 20 min, a white precipitate formed (AgCl) and the solution turned light yellow. The reaction was stirred at room temperature for 2 h. Meanwhile, in another Schlenk flask, **1** (50 mg, 0.10 mmol) was dissolved in acetone (5 mL) and 2 equiv of Cs_2CO_3 (65.8 mg, 0.20 mmol) was added at once. The reaction was stirred for 2 h. The filtered light-yellow solution of $[(ppy)_2Ir(solvent)_2]^+$ was added to a suspension of [Cs][Cp*Ru(catecholate)] and stirred for an additional 1 h. Then the solvent was removed under vacuum, and the residue was dissolved in CH_2Cl_2 and filtered through alumina. Evaporation of CH_2Cl_2 under vacuum provided the bimetallic complex as an orange solid (51 mg, 60% yield). ^1H NMR (300 MHz, CD_2Cl_2): δ 9.09 (d, 1H, J = 5.5 Hz, H ppy), 8.71 (d, 1H, J = 5.0 Hz, H ppy), 7.89 (d, 1H, J = 8.6 Hz, H ppy), 7.78 (m, 2H, H ppy), 7.63 (m, 2H, H ppy), 7.52 (d, 1H, J = 7.3 Hz, H ppy), 7.31 (t, 1H, J = 6.3 Hz, H ppy), 7.06 (t, 1H, J = 6.3 Hz, H ppy), 6.79 (m, 2H, H ppy), 6.63 (m, 2H, H ppy), 6.22 (d, 1H, J = 7.5 Hz, H ppy), 6.08 (d, 1H, J = 7.5 Hz, H ppy), 4.95 (d, 1H, J = 5.4 Hz, H π-arene), 4.87 (d, 1H, J = 5.4 Hz, H π-arene), 4.42 (m, 2H, H π-arene), 1.70 (s, 15H, CH_3 Cp*). IR (ATR, cm^{-1}): 3234, 3037, 2966, 2902, 1697, 1602, 1508, 1465, 1413, 1381, 1345, 1298, 1263, 1223, 1158, 1029, 992, 823, 792, 754, 728, 668, 629, 616, 597, 532, 472, 447, 420, 380, 350, 326. Anal. Calcd for $C_{38}H_{35}IrN_2O_2Ru$ (844.98 g·mol^{-1}): C, 54.01; H, 4.17. Found: C, 53.99; H, 4.65.

dx.doi.org/10.1021/ic202021w | Inorg. Chem. 2012, 51, 1739−1750

X-ray Crystal Structure Determination of 5-OTf, 8, and 11. A single crystal of compound **5**-OTf, **8**, or **11** was selected, mounted onto a glass fiber, and transferred in a cold-nitrogen gas stream. Intensity data were collected with a Bruker Kappa-CCD or Kappa-APEX2 with graphite-monochromated Mo Kα radiation. Unit-cell parameter determination, data collection strategy, and integration were carried out with the *EVAL-14*[28] or *APEX2* suite of programs. Multiscan absorption correction was applied.[29] The structures were solved by direct methods using the *Sir92*[30] or *SUPERFLIP*[31] programs. Almost all non-H atoms were refined anisotropically. All H atoms were placed at calculated positions. In **5**-OTf, the triflate anions were refined isotropically. One OTf anion is disordered over two positions (0.6/0.4 site occupation factors), and its geometry was restrained. The second anion showed quite important isotropic thermal parameters, but no sensible model of disorder could be obtained. In **8**, there is nonnegligible (and nonmodelized) residual density near the Rh1 atom (0.97 Å) that prevented the anisotropic refinement of the neighboring N atom.

These data can be obtained free of charge from The Cambridge Crystallographic Data Centre via www.ccdc.cam.ac.uk/data_request/cif.

Crystal data for **5**-OTf (CCDC 790660): purple crystals, $C_{37}H_{36}F_3N_4O_{5.5}Ru_2S$, triclinic, $P\bar{1}$, a = 14.337(2) Å, b = 15.2172(11) Å, c = 18.279(3) Å, α = 103.270(10)°, β = 92.249(12)°, γ = 100.276(10)°, V = 3805.7(9) Å^3, Z = 4, T = 200(2) K, μ = 0.911 mm^{-1}, 66 434 reflections measured, 17 175 independent (R_{int} = 0.0752), 9080 observed [$I > 2\sigma(I)$], 906 parameters, final R indices R1 [$I > 2\sigma(I)$] = 0.0750 and wR2 (all data) = 0.2501, GOF on F^2 = 1.054, max/min residual electron density = 1.85/−1.86 e·Å^{-3}.

Crystal data for **8** (CCDC 810215): light green crystals, $C_{155}H_{152}Cl_6N_8O_{11}Rh_4Ru_4$, triclinic, $P\bar{1}$, a = 12.9964(17) Å, b = 23.346(3) Å, c = 23.532(5) Å, α = 99.441(10)°, β = 96.782(13)°, γ = 95.373(10)°, V = 6947.2(19) Å^3, Z = 2, T = 200(2) K, μ = 1.065 mm^{-1}, 106 575 reflections measured, 30 112 independent (R_{int} = 0.0767), 16 028 observed [$I > 2\sigma(I)$], 1691 parameters, final R indices R1 [$I > 2\sigma(I)$] = 0.0716 and wR2 (all data) = 0.2088, GOF on F^2 = 1.056, max/min residual electron density = 6.80/−2.99 e·Å^{-3}.

Crystal data for **11** (CCDC 807111): orange crystals, $C_{40}H_{39}Cl_4IrN_2O_2Ru$, orthorhombic, $P2_12_12_1$, a = 12.5121(3) Å, b = 14.5305(4) Å, c = 21.4119(6) Å, V = 3892.83(18) Å^3, Z = 4, T = 200(2) K, μ = 4.114 mm^{-1}, 38 729 reflections measured, 11 659 independent (R_{int} = 0.0230), 10 538 observed [$I > 2\sigma(I)$], 456 parameters, final R indices R1 [$I > 2\sigma(I)$] = 0.0232 and wR2 (all data) = 0.0600, GOF on F^2 = 1.013, max/min residual electron density = 0.88/−0.71 e·Å^{-3}.

Optical Spectroscopy. Solvents used for photophysical determinations were spectroscopic grade (C. Erba). Molar absorptivity values (ε) were calculated by applying the Beer−Lambert law to low-absorbance spectra (A < 1) of complexes recorded at successive dilutions by using a Perkin-Elmer Lambda 950 UV−visible−NIR spectrophotometer. Steady-state photoluminescence spectra were measured on sample solutions with A < 0.1 at the excitation wavelength in right-angle mode by using a Spex Fluorolog II spectrofluorimeter, equipped with a Hamamatsu R928 phototube. Corrected spectra were employed throughout this work by applying to the raw data a correction curve of the wavelength-dependent phototube response between 280 and 900 nm obtained by using a calibrated halogen-lamp source. Quartz capillary tubes immersed in liquid nitrogen in a coldfinger quartz dewar were used for the measurement of MeOH/EtOH (1:4) frozen glasses at 77 K. Nanosecond laser flash photolysis experiments were performed by a system based on a Nd:YAG laser (JK Lasers, 355 nm, 4.0 mJ/pulse, 18 ns pulse) using a right-angle analysis on the excited sample, previously described.[32] The samples were bubbled with argon for ca. 15 min and sealed in homemade 10-mm-optical-path-length cells. Luminescence lifetimes were measured with an IBH 5000F time-correlated single-photon-counting apparatus, by using a pulsed NanoLED excitation source at λ = 373 nm. Analysis of the luminescence decay profiles against time was accomplished with the Decay Analysis Software DAS6 provided by the manufacturer. Experimental uncertainties are estimated to be 2 nm on band maxima and 10% in the lifetime determination.

Theoretical Calculations. The *GAUSSIAN 09*[33] program package was used to perform DFT[34] and TD-DFT[35] calculations. The singlet ground-state geometries of the nine complexes **5**−**13** were optimized using the exchange-correlation functional PBE0[36] in vacuo. Effective core potentials (ECPs) were used to account for the inner-shell electrons of the transition metals. Particularly, the small-core relativistic energy-consistent pseudopotentials (PPs) of the Stuttgart/Cologne group were employed, along with their correlation-consistent basis sets of double-ζ quality for the 4d Ru and Rh (ECP28MDF/VDZ basis set),[37] and 5d Ir (ECP60MDF/VDZ basis set)[38] transition metals. The peculiarity of these PPs is that they incorporate both scalar and spin−orbit relativistic effects and are expected to be definitely more appropriate to describe the transition metals, particularly when relativistic effects are large. The 6-31G* basis set[39] was employed for all of the other atoms. The accuracy of the calculated geometries was tested by comparison with the X-ray diffraction (XRD) available data for **5**-OTf and **7**-OTf$_2$.[18a] The calculations of the Hessian matrices for all complexes confirm that the geometries are those corresponding to the minimum on each potential energy surface with harmonic frequencies ranging from 13 to 20 cm^{-1}. To assign the spectral region above 300 nm, the first 33 singlet−singlet excited-state transitions of **5**−**7** were calculated by TD-DFT using the hybrid meta exchange-correlation functional M06 of Zhao and Truhlar.[40] In the case of complexes **8**−**13**, the calculation of only 24 transitions is enough to cover the investigated range of wavelengths. In order to compare the calculated spectra with the absorption spectra in a CH_2Cl_2 solution, the default integral equation formalism (IEFPCM) variant of the polarizable continuum model (PCM)[41] was used to account for solvation. The simulations of the electronic spectra were obtained by summing up Gaussian functions centered at each calculated wavelength with the high of the maxima related to the oscillator strength. A full width at half-maximum (fwhm) of 60 nm was found adequate to satisfactorily reproduce the low-energy region of the spectra. The electron density plots of the lowest triplet states of **9** and **10**, reported in the Supporting Information, were calculated using the procedure followed in the case of the singlet state specified above, accounting for the different multiplicities at every stage of the computations. The electron density plots were drawn by using *MOLDEN*.[42]

RESULTS AND DISCUSSION

Synthesis and Characterization of the OM-Linkers 2−4. The syntheses of *o*-benzoquinone complexes of rhodium and iridium [Cp*M(*o*-benzoquinone)]: M = Rh (**3**); M = Ir (**4**) were previously reported by us.[18a] They involve the π complexation of catechol in acetone in the presence of excess $BF_3{\cdot}2H_2O$ to give the π-bonded catechol complexes [Cp*M-(η^6-$C_6H_6O_2$)][BF_4]$_2$. Subsequent deprotonation with Cs_2CO_3 in acetone afforded the target π-bonded OM-linkers **3** and **4**. The presence of trifluoroborane is important to allow placement of the metal center to the π ring and avoid OO coordination of the catechol to the metal center, as observed previously by Maitlis et al.[43] However, we note that π-bonded quinonoid complexes of "Mn(CO)$_3$" were described.[44] As for the *o*-benzoquinone complex of ruthenium **2**, it involves a slightly different procedure. The first step consists of the treatment of catechol in CH_2Cl_2 with air-sensitive [Cp*Ru-(CH_3CN)$_3$][OTf] to give the air-stable π-bonded catechol complex [Cp*Ru(η^6-$C_6H_6O_2$)][OTf] (**1**).[45] The ^{1}H NMR spectrum of **1** recorded in CD_2Cl_2 showed a singlet at δ 1.90 assigned to the Cp*Ru unit and two sets of multiplets at δ 5.21 and 5.80 attributed to the π ring of the coordinated catechol. The phenolic protons are also visible and appear as a broad singlet at δ 7.99. Complex **1** was then treated with Cs_2CO_3 for 16 h subsequent to the reaction workup, providing the OM-

dx.doi.org/10.1021/ic202021w | Inorg. Chem. 2012, 51, 1739−1750

linker **2**-Cs as an off-white microcrystalline powder, which is very moisture-sensitive. The ^{1}H NMR spectrum of **2**-Cs recorded in CD_2Cl_2 showed an upfield shift relative to the parent molecule **1** notably for the protons of the carbocycle ring. For instance, complex **2**-Cs showed two sets of multiplets at δ 4.74 and 5.07, and the singlet for the Cp*Ru unit appears now at δ 1.80.

Preparation and Characterization of the Coordination Assemblies with OM-Linkers. The syntheses of the binuclear assemblies (**6**-**7**)-OTf, (**9**-**10**)-OTf, and (**12**-**13**)-OTf with the neutral rhodium and iridium OM-linkers [Cp*M(o-$C_6H_4O_2$)] [M = Rh (**3**), M = Ir (**4**)] were recently reported.[18a,46] The related salts **7**-ΔT, **10**-ΔT, and **13**-ΔT with Δ-TRISPHAT as the counteranion were obtained from anion metathesis through elution of the starting material with CH_2Cl_2 in the presence of [cinchonidinium][Δ-TRISPHAT][47] (Figure 1) on a neutral alumina column.

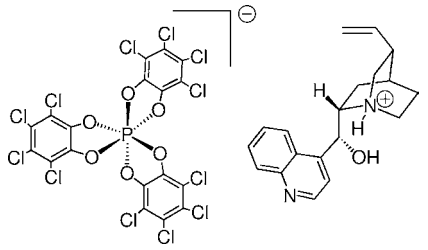

Figure 1. Schematic drawing of [cinchonidinium][Δ-TRISPHAT].

In a similar approach, the novel homo- and heterobinuclear assemblies **5**-OTf, **8**, and **11** were obtained by treatment of the anionic ruthenium OM-linker **2**-Cs with luminophore bricks such as "$(bpy)_2Ru(II)^{2+}$", "$(ppy)_2Rh(III)^{+}$", and "$(ppy)_2Ir(III)^{+}$" (bpy = 2,2′-bipyridine; ppy = 2-phenylpyridine) in acetone. For instance, the treatment of **2**-Cs with the solvated brick $[(bpy)_2Ru(acetone)_2][OTf]_2$ prepared in situ in acetone for 1 h, followed by the reaction workup, provided a deep burgundy microcrystalline material identified by spectroscopic data and elemental analysis as **5**-OTf. The ^{1}H NMR spectrum of **5**-OTf recorded in CD_2Cl_2 presented 14 multiplets in a range of δ 6.98 and 9.33 corresponding to the two nonequivalent bpy ligands, three multiplets at δ 4.45, 4.83, and 4.99, which are attributed to the π-coordinated o-$C_6H_4O_2$, and a singlet at δ 1.64 for η^5-Cp*Ru. Interestingly, the latter signals are upfield relative to the free OM-linker **2**-Cs. These data are in contrast to those observed generally with the binuclear octahedral assemblies (**6**-**7**)-OTf, (**9**-**10**)-OTf, and (**12**-**13**)-OTf, displaying the neutral OM-linkers **3** and **4**.

We then decided to prepare the related complex [$(bpy)_2$Ru(**2**)][Δ-TRISPHAT] (**5**-ΔT) with Δ-TRISPHAT as the counteranion instead of triflate. The idea to study the luminescent properties of a series of binuclear assemblies with Δ-TRISPHAT is to probe whether a novel property might arise from possible ion-paired complexes in solution or in the solid state with the Δ-TRISPHAT. For instance, Thompson and co-workers examined the photophysical properties of some ion-paired iridium complexes and their applications in organic light-emitting devices.[48] In our case, the chiral anion, "not the OM anion as in the precedent example", tends to form ion-paired complexes as supported by several X-ray molecular structures.[49] For instance, the X-ray molecular structure of the dinuclear ruthenium complex *trans*-[(Sp,Sp)-bis(Cp*Ru)-carbazolyl][Δ-TRISPHAT], which possesses a planar chirality, showed two $\pi-\pi$ interactions between one of the tetrachlorobenzene rings of Δ-TRISPHAT and the two η^5-Cp*Ru units of two cationic metal complexes with d_1 = 3.51 and d_2 = 3.66 Å, respectively. As a result, the Δ-TRISPHAT anion intercalates between two cationic complexes, providing a one-dimensional supramolecular chain.[50] Complex **5**-ΔT was prepared by mixing **5**-OTf with an excess of [cinchonidinium][Δ-TRISPHAT] and eluted on a column of neutral alumina with CH_2Cl_2. The target compound **5**-ΔT was obtained in 70% yield as a dark-purple microcrystalline solid. The ^{1}H NMR spectrum recorded in CD_2Cl_2 showed a pattern similar to that of **5**-OTf; however, all signals appeared broad, reminiscent of the presence of a mixture of the two diastereomers [Δ-$(bpy)_2$Ru(**2**)][Δ-TRISPHAT] (**5Δ**-ΔT) and [Λ-$(bpy)_2$Ru(**2**)][Δ-TRISPHAT] (**5Λ**-ΔT). The elemental analysis is in accordance with the proposed formula. The luminescence properties were carried out on both species without separation of the two compounds. To complete this series, we then decided to prepare the neutral binuclear compounds with luminophore bricks $[M(ppy)_2]^+$ (M = Rh, Ir). Thus, the treatment of **2**-Cs prepared in situ with $[(ppy)_2Rh(acetone)_2][OTf]$ in acetone for 1 h at room temperature provided a yellow-greenish solution. Reaction workup allowed isolation of the target compound **8** in 76% yield as a light-green microcrystalline solid. The related heterobinuclear species **11** was obtained in 60% yield as an orange microcrystalline solid. Spectroscopic data (^{1}H and ^{13}C NMR and IR) were in accordance with the proposed formulas (see the Experimental Section); moreover, the X-ray molecular structure of **11** was identified without ambiguity.

X-ray Molecular Structures of 5-OTf, 8, and 11. Suitable crystals of the three compounds were grown at room temperature by the slow diffusion of diethyl ether into a CH_2Cl_2 solution. Crystals of **5**-OTf are purple, those of **8** are light green, and those of **11** are orange. The molecular structures of **5**, **8**, and **11** are shown in Figure 2. Comparative bond distances and angles are depicted in Table 1. The X-ray structure of **5**-OTf revealed the presence of two independent molecules, a and b, and confirmed the O^O′ chelating mode of the OM-linker **2** to the $Ru(bpy)_2$ core via both O atoms. The Ru^{II} center is also coordinated to four N atoms of two bpy ligands, which describe a distorted octahedral geometry around the metal center. The structure also shows that the carbocycle ring is coordinated to the "Cp*Ru" moiety via the four diene C atoms in an η^4 fashion; the Ru2---C21 and Ru2---C22 distances are 2.31 and 2.41 Å, respectively, indicating the absence of interaction. The two quinone functional groups are bent upward relative to the Cp*Ru moiety with only 5.98°; this angle is smaller than that reported previously for the octahedral assembly [$(bpy)_2$Ru(**4**)][OTf]$_2$ (**7**-OTf), where θ = 12.74°. Further, the C21---O1 and C22---O2 bond distances are of 1.326 and 1.310 Å. These data are consistent with the C---O length found in the *semiquinone form* in a large number of dioxelene complexes.[19a,51] The C21---C22 bond length within the chelate ring is of 1.42 Å, also suggesting the presence of a *semiquinone form* of the carbocycle ring. The related neutral iridium complex **11** featured only one single molecule in the unit cell. The structure shows that the OM ligand **2** chelates the $Ir(ppy)_2$ moiety via both O atoms through a O^O′ coordination mode, as shown in the previous example. The Ir^{III} center is also coordinated to two phenylpyridine ligands with cis-metalated C atoms and trans-metalated N atoms, as expected for these types of $L_2Ir(ppy)_2$ complexes and thus describing a distorted

dx.doi.org/10.1021/ic202021w | *Inorg. Chem.* 2012, 51, 1739–1750

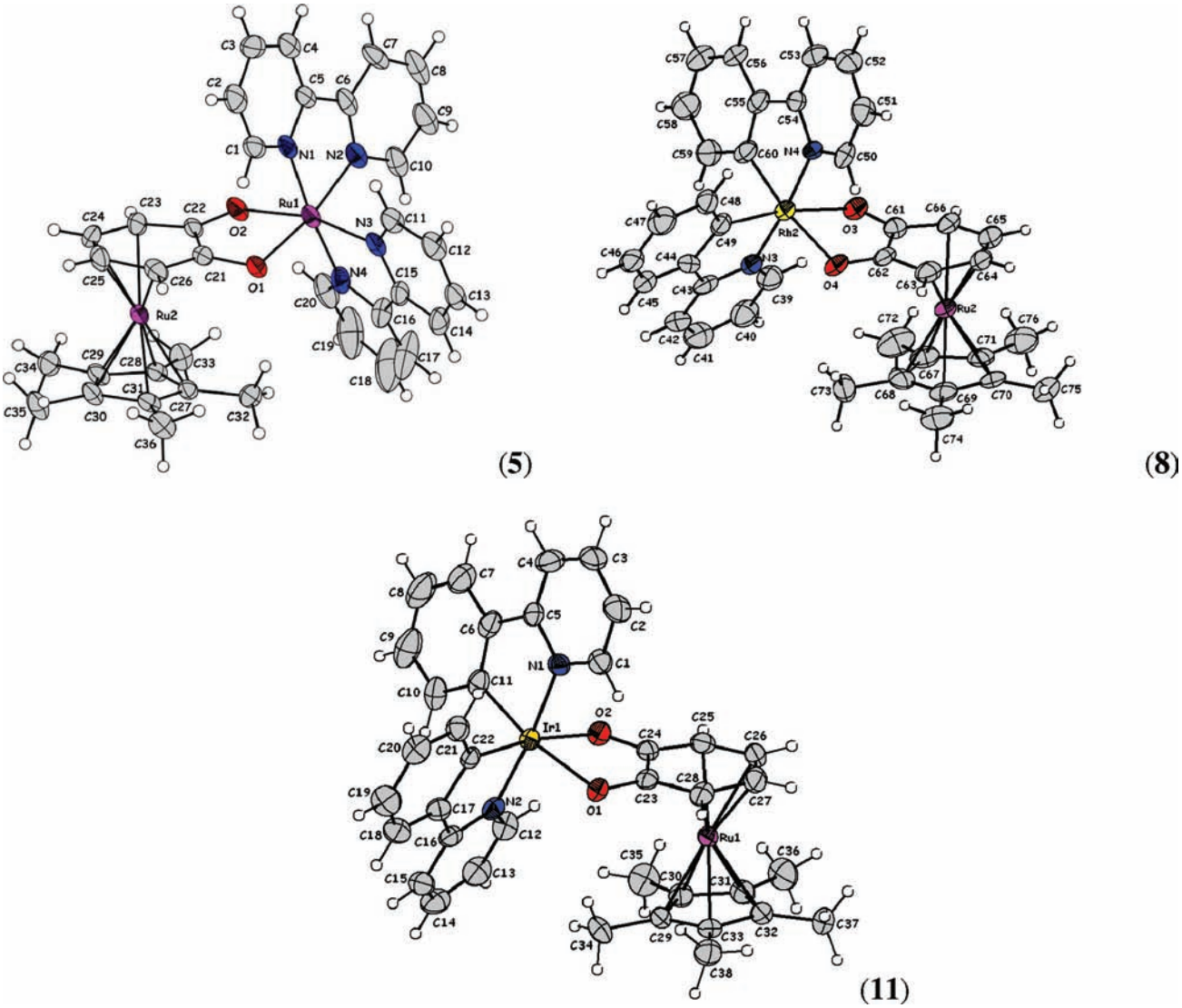

Figure 2. Molecular structures of **5** and the neutral species **8** and **11** at 30% ellipsoids with atom labeling.

octahedral geometry. The Ir−N bond distances in the pyridyl moiety of the two chelating C^N ligands are about 2.017 and 2.035 Å, while those of the phenyl ring Ir−C are about 1.981 and 1.991 Å. These bond distances are shorter than those reported for $L_2Ir(ppy)_2$ compounds. The structure reveals that the carbocycle ring is coordinated to Cp*Ru through only four C atoms in an η^4 fashion; the Ru1---C23 and Ru1---C24 distances are 2.359 and 2.425 Å, respectively, indicating the absence of interaction. The two quinone functional groups are almost planar relative to the Cp*Ru-ring moiety with only 6.29°; this angle is comparable to that found for **5**-OTf but smaller than that reported previously for the octahedral assembly 7-OTf, where θ = 12.74°. Moreover, the C23---O1 and C24---O2 bond distances of 1.311 and 1.295 Å are similar to those found for **5**-OTf and 7-OTf[18a] and are consistent with the C---O length found in dioxelene−metal complexes displaying a *semiquinone form*. Moreover, the C23---C24 bond distance is 1.442 Å, comparable to that found in the previous complex. The X-ray molecular structure of the rhodium complex **8** revealed the presence of four independent molecules. The structure of one of these molecules is depicted in Figure 2 and showed similar features relative to the iridium congener **11**. The structure shows that the anionic OM-linker **2** chelates the $Rh(ppy)_2^+$ luminophore brick via both oxygen centers through O^O′ coordination mode. In this dinuclear assembly, the two quinone functional groups form an angle θ = 6.76° with respect to the rest of the carboxy ring. This value is slightly bigger than that found for complex **5**-OTf but smaller than that reported for **7**-OTf and comparable with the congener iridium species **11**. Further, the C−O bond distances of the two carbonyl functions C61---O3 and C62---O4 are 1.31 and 1.29 Å, similar to those found for the iridium congener and those found for the monocationic **5**-OTf and dicationic **7**-OTf related complexes; moreover, the C61---C62 bond distance is 1.44 Å. As in the case of the iridium congener **11**, these bond distances compare well with those found for dioxelene−metal complexes displaying a *semiquinone form*. In summary, the above structural comparisons among these novel families of octahedral metal complexes displaying metalated quinonoid ligands show that the *quinone form* of the coordinated OM-linker loses its structure upon moving from a dicationic species to a monocationic one and finally the neutral rhodium and iridium species, which display more *catecholate resonance* structures compared to these metalated dioxolene ligands.

dx.doi.org/10.1021/ic202021w | *Inorg. Chem.* 2012, 51, 1739−1750

Table 1. Comparative Bond Distances (Å) and Angles (deg) for Complexes 5, 8, and 11

	5	8	11
	Bond Lengths		
C---O	C21---O1: 1.326(8)	C61---O3: 1.31(1)	C23---O1: 1.311(4)
	C22---O2: 1.31(1)	C62---O4: 1.29(1)	C24---O2: 1.295(4)
C---C	C21---C22: 1.42(2)	C61---C62: 1.44(1)	C23---C24: 1.442(4)
M---C(diene)	Ru2---C23: 2.24(1)	Ru2---C63: 2.17(1)	Ru1---C25: 2.236(3)
	Ru2---C24: 2.18(1)	Ru2---C64: 2.17(1)	Ru1---C26: 2.180(4)
	Ru2---C25: 2.17(1)	Ru2---C65: 2.17(1)	Ru1---C27: 2.168(4)
	Ru2---C26: 2.17(1)	Ru2---C66: 2.23(1)	Ru1---C28: 2.191(4)
M---X(bpy or ppy) (X = C, N)	Ru1---N1: 2.054(8)	Rh2---N3: 2.010(8)	Ir1---N1: 2.035(3)
	Ru1---N2: 2.021(9)	Rh2---N4: 2.050(8)	Ir1---N2: 2.017(3)
	Ru1---N3: 2.026(6)	Rh2---C49: 1.965(8)	Ir1---C11: 1.981(4)
	Ru1---N4: 2.008(7)	Rh2---C60: 1.97(1)	Ir1---C22: 1.991(3)
	Bond Angles		
O–M–O	O1–Ru1–O2: 80.3(2)	O3–Rh2–O4: 77.0(2)	O1–Ir1–O2: 77.81(9)
N–M–N	N1–Ru1–N2: 79.3(3)		
	N3–Ru1–N4: 79.2(3)		
N–M–C		N3–Rh2–C49: 81.0(3)	N1–Ir1–C11: 80.6(1)
		N4–Rh2–C60: 82.1(3)	N2–Ir1–C22: 81.2(1)

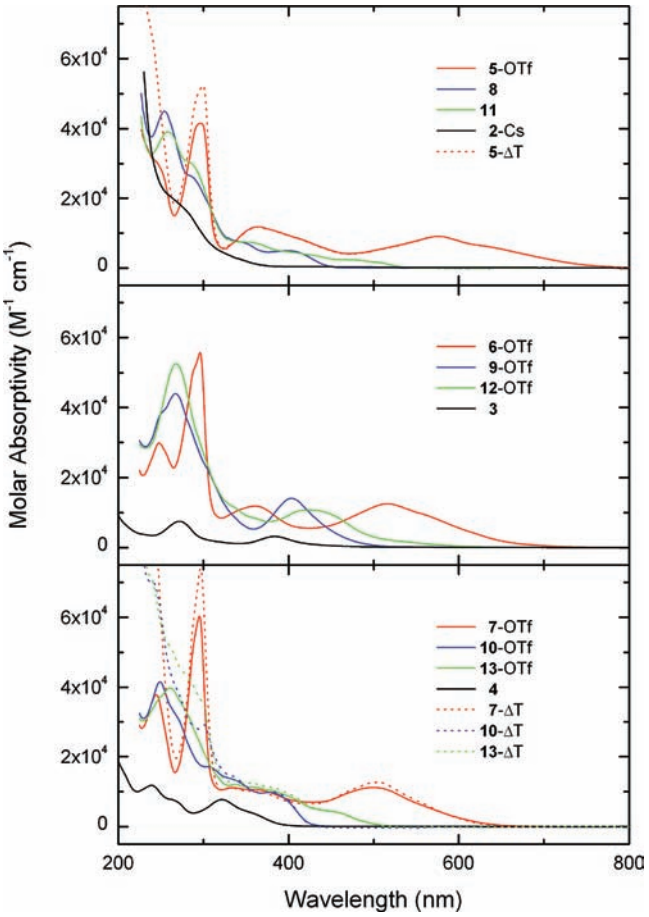

Figure 3. Absorption spectra of complexes **2** and **5**–**13** in a CH_2Cl_2 solution and of complexes **3** and **4** in a CH_3OH solution.

All in all, these examples are the first to be described for metalated dioxelene ligands coordinated to luminophore bricks. Lever et al. described the syntheses of a variety of dioxelene–metal complexes displaying *semiquinone form*. The latter show a typical NIR absorption in the 1000–1200 nm region related to the semiquinone fashion. In contrast, our compounds, although the solid-state structures argue in favor of a *semiquinone form*, are not paramagnetic in solution and do not exhibit such an absorption (vide infra). We propose that the presence of the metal in these dioxolene ligands profoundly modifies the electronic properties of the examined octahedral complexes with OM ligands. Their absorption and luminescence features are described in the next sections.

Absorption. The absorption spectra of the binuclear complexes recorded in CH_2Cl_2 and CH_3OH solutions are reported in Figure 3, and relevant data are collected in Table 2. The absorption profiles of the investigated binuclear [Rh(ppy)$_2$(**2**–**4**)] and [Ir(ppy)$_2$(**2**–**4**)] derivatives, **8**–**10** and **11**–**13**, respectively, show a similar envelope of high-energy electronic transitions (Figure 3) in the spectral region of 240–310 nm. They originate from spin-allowed $^1\pi,\pi^*$ ligand-centered (^{1}LC) transitions of the phenylpyridine ligands, with some likely contribution from ^{3}LC forbidden transitions,[52] enabled by the heavy-atom effect of the iridium and rhodium nuclei (ζ_{Rh} = 1259 cm^{-1}; ζ_{Ir} = 3909 cm^{-1}).[53]

The low-energy absorption bands present at 350–500 nm in the spectra of **8**, **10**, **11**, and **13** OTf derivatives are of less straightforward attribution. In fact, the usual assumption used to interpret the spectroscopic properties of inorganic complexes, i.e., that both the ground and excited states can be described by a localized molecular orbital (MO) configuration, is less applicable in OM compounds, where a large degree of covalency in the metal–C$^-$ σ bonds exists. On this basis, for the above-mentioned rhodium and iridium binuclear complexes, it seems reasonable to consider for these low-intensity absorption features ($\varepsilon \approx 10\,000$ mol^{-1}·L·cm^{-1}) not only ^{1}MLCT transitions related to the iridium(III) and rhodium(III) phenylpyridyl moieties[52a] but also CT transitions from the occupied d metal orbitals to the π^* MOs of the metalated dioxelene moiety, either of σ bond to ligand charge transfer (^{1}SBLCT) or mixed ^{1}MLCT/intravalent charge-tranfer (^{1}ILCT) character.[54] The **9**-OTf and **12**-OTf complexes, instead, show a clearly defined low-energy absorption band (peaking at 424 nm in **12**-OTf and at 404 nm in **9**-OTf; Table 2). This indicates an influence of the metal present in the OM-linker on the distribution of the CT transitions originating from the iridium and rhodium metals sitting in the octahedral coordination environment. The bimetallic ruthenium derivatives **5**–**7** exhibit quite different spectral shapes. Their absorption spectra display three main features, in order of decreasing energy: (i) an intense band in the UV region of the spectrum, located around 290 nm, which is usually assigned to bpy-centered π,π^* transitions;[55] (ii) a middle-energy band at ca. 360 nm, with absorption coefficients larger than 10^4 mol^{-1}·L·cm^{-1}; (iii) a low-intensity, low-energy band, whose energy is modulated by the metal in the OM-linker (**2**–**4**). This

dx.doi.org/10.1021/ic202021w | Inorg. Chem. 2012, 51, 1739–1750

Table 2. Photophysical Parameters of the Examined Complexes

	absorption (room temperature)[a]	emission (77 K)[b]	
	λ_{max}/nm (ε_{max}/M^1·cm^{-1})	λ_{max}/nm	τ/μs
5-OTf	247 (29 900), 297 (41 600), 363 (11 900), 578 (9000)	765	1.2
5-ΔT	299 (52 400), 364 (11 800), 578 (9000)	765	1.1
6-OTf	248 (29 800), 296 (55 800), 362 (11 800), 517 (12 500)	692	1.1
7-OTf	245 (31 500), 295 (50 300), 356 (10 600), 501 (9300)	698	1.3
7-ΔT	297 (73 900), 355 (10 100), 505 (12 700)	698	1.2
8	254 (45 000), 288 (26 000), 346 (7400), 402 (4900)	466	96
9-OTf	253 (39 000), 267 (43 900), 305 (22 100), 404 (14 100)	460	96
10-OTf	249 (41 600), 301 (17 200), 336 (13 400), 378 (9800)	460	95
10-ΔT	239 (70 500), 301 (29 100), 332 (14 700), 381 (9900)	459	94
11	258 (39 100), 286 (30 100), 350 (7400), 474 (2400)	515	5.0
12-OTf	268 (52 600), 424 (10 700)	486	5.1
13-OTf	261 (39 800), 282 (31 900), 350 (11 400), 450 (4300)	487	4.9
13-ΔT	280 (43 500), 356 (12 400), 455 (4300)	488	4.8
2	270sh (18 800)		
3	272 (7500), 383 (3200)[c]		
4	239 (11 800), 321 (7700), 360sh (3700)[c]		

[a]In a CH_2Cl_2 solution. [b]In a MeOH/EtOH (1:4, v/v) mixture; excitation at 373 nm. [c]In a MeOH solution.

low-energy absorption band has been assigned to the $d_{Ru}-\pi^*_{bpy}$ transition of $ML_{bpy}CT$ character with minor contributions from $\pi_{bzq}-\pi^*_{bpy}$ transitions of $L_{bzq}L_{bpy}CT$ character.[26] The monometallic benzenedionecyclopentadienyl derivatives **3** and **4** show an envelope of moderate-intensity ($\varepsilon \approx 10\,000$ mol^{-1}·L·cm^{-1}) absorption transitions in the UV portion of the spectrum, centered around 240 and 270 nm for **4** and **3**, respectively, which are associated with the cyclopentadienyl−metal subunit.[56] The lower-intensity bands ($\varepsilon \approx 3000-7000$ mol^{-1}·L·cm^{-1}) extending from 300 to 500 nm, which are absent in complex **2**, are most likely associated with the benzenedione−metal subunit, and from the magnitude of the extinction coefficient, the transitions are probably charge transfer in character.

TD-DFT Calculation of Excitation Spectra. To gain deeper insight into the character of the excitations that give rise to the observed absorption spectra of **5**−**13**, they were calculated by means of TD-DFT using the M06 hybrid meta exchange-correlation functional, recommended by Zhao and Truhlar[40] for application in OM chemistry. PPs and basis sets that account for the relativistic effects of the transition metals were employed,[37,38] and the complexes were considered in a CH_2Cl_2 solution by means of the PCM.[41] The geometries used are those of the nine complexes calculated in vacuo by the PBE0[36] hybrid functional because preliminary tests and a comparison with the XRD available structures of **5** and **11** indicated its adequateness in accurately calculating them. The analysis of the absorption spectra relies on the information of the excitations characterizing each transition and on the electron density plot of the MOs of **5**−**13**, which are reported in the Supporting Information along with the calculated energies/wavelengths and oscillator strengths of the singlet−singlet transitions. An example of the calculated frontier orbitals is reported in Figure 4 for **5**−**7**. Examination of the electron density distribution of these complexes indicates that it is ruled by the kind of OM-linker within the complex. In **5**, **8**, and **11**, where the OM-linker with ruthenium is present, the benzoquinone ring significantly participates in the description of the highest occupied MOs (HOMOs). On the contrary, the OM-linkers with rhodium and iridium only contribute to the HOMO−1 of **9**, **10**, **12**, and **13**, with the electron densities of

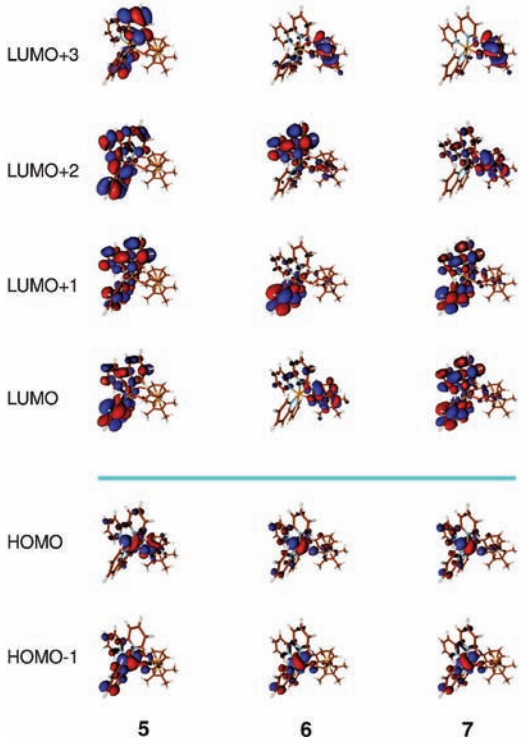

Figure 4. Electron density plots calculated for the bimetallic complexes **5**−**7**.

the other HOMOs being largely localized on the $Rh(ppy)_2$ and $Ir(ppy)_2$ moieties, whereas the HOMOs of $Ru(bpy)_2$ complexes **6** and **7** closely resemble those of **5** (Figure 4). Moreover, the complexes with the Ru-linker (**5**, **8**, and **11**) differentiate from the others because of their low-energy virtual MOs, which are completely characterized by the bpy (**5**) and ppy (**8** and **11**) ligands. In fact, in all of the other complexes, the electron density distribution of some of these MOs is also localized over the OM-linkers, besides the bpy and ppy ligands. This and the fact that most of the calculated transitions have a multiconfigurational character, describing excitations involving both the ligands and OM-linkers, evidence that the assignment

dx.doi.org/10.1021/ic202021w | Inorg. Chem. 2012, 51, 1739−1750

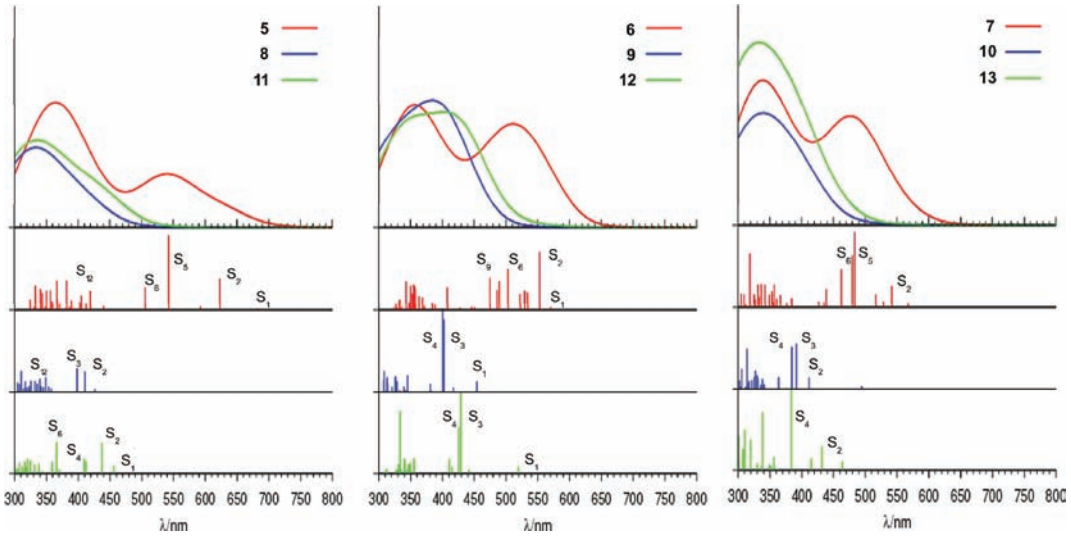

Figure 5. Simulated absorption spectra (upper) and calculated oscillator strengths (lower) for the bimetallic complexes **5**−**13**.

of the absorption bands performed in terms of excitations characterized by MOs localized on the different moieties gives a limited description of the character of the transitions of these complexes.[57] With this in mind, the assignment of the absorption spectra focuses on the main contributions by singlet−singlet excitations, relying on the familiar description given by the localized MOs. More details of each calculated transition are included in the Supporting Information.

The simulations of the absorption spectra, reported in Figure 5, satisfactorily reproduce the spectral features of the absorption bands above 300 nm observed in the bimetallic complexes (Figure 3). The absorption spectra of the $Ru(bpy)_2$ derivatives **5**−**7** show a characteristic broad absorption band at low energy followed by another absorption at higher energy. In the case of **5**, the first absorption band (λ > 500 nm) originated by transitions to the first six excited states ($S_0 \rightarrow S_1$−S_6), which are characterized only by excitations starting from the three HOMOs to the three LUMOs, thus assigned to Ru → bpy transitions. In the spectral region 300−420 nm, excitations starting from the inner occupied MOs, largely characterized by the OM-linker, become more and more significant with increasing energy. On the whole, these absorptions can be assigned to OM-linker → bpy transitions. A similar assignment is performed for **6** and **7**, which feature the rhodium and iridium OM-linkers, respectively, where the low-energy absorption band is blue-shifted with respect to that of **5** and more transitions (up to $S_0 \rightarrow S_{10}$) contribute to its intensity. Nevertheless, in this case, the description of the final states also accounts for contributions by low-lying virtual MOs, whose electron density is spread over the OM-linker. The transitions to the higher-energy absorption band (~320−420 nm) of **6** and **7** originate from the same set of MOs and end up to higher virtual MOs. Besides, excitations starting from inner MOs with electron density distributed over the OM-linker contribute to the high-energy part of these bands. The low-energy absorption bands of both $Rh(ppy)_2$ (**8**−**10**) and $Ir(ppy)_2$ (**11**−**13**) derivatives are significantly blue-shifted with respect to those of $Ru(bpy)_2$ derivatives (**5**−**7**). All in all, the multiconfigurational description of the first three excited states indicates that the excited electron is initially delocalized all over the complex and ends up on ppy-centered virtual MOs in the case of **8** and **11**, which have the ruthenium OM-linker. Thus, the low-energy band in both cases can be attributed to CT transitions toward the ppy ligands, with mixed MLCT and LLCT character. In the cases of **9**, **10**, and **12**, the weak transition to the first excited state is assigned to $M(ppy)_2$ → OM-linker, while those to the other low excited states contain contributions by OM-linker → OM-linker transitions. Among them, particularly intense are the calculated $S_0 \rightarrow S_3$ and $S_0 \rightarrow S_4$ transitions. The first three excited states of **13** of weak intensity are assigned to MLCT transitions, while the intense $S_0 \rightarrow S_4$ transition is mainly characterized by HOMO−1 → LUMO excitation with OM-linker → ppy character. In all cases, the MLCT and LLCT character increases in transitions to higher excited states. More difficult is the attribution of the higher-energy part of these absorption bands in the examined range of wavelengths because the calculated transitions are characterized by multiconfigurational descriptions that include more and more excitations, which account for electron densities widely delocalized on the whole complex. Thus, the simple assumption frequently used to interpret the spectroscopic properties of inorganic complexes, i.e., that both the ground and excited states can be described by a localized MO configuration, is not applicable for these kinds of complexes. The low-energy tail observed in the $Ir(ppy)_2$ derivatives **11**−**13** and absent in $[Rh(ppy)_2(\mathbf{2}-\mathbf{4})]^+$ is not accounted for by the model. This includes direct singlet-to-triplet excitations of spin-forbidden character, induced by the large spin−orbit coupling constant of the Ir atom.

Emission. The normalized luminescence spectra obtained at 77 K in a 1:4 MeOH/EtOH mixture are reported in Figure 6, and the relevant photophysical parameters are summarized in Table 2. All examined complexes are poorly or nonemissive at room temperature in deaerated solutions ($\phi \approx 10^{-4}$−10^{-5}). In contrast with the room temperature behavior, all of the binuclear complexes were found to intensely luminesce at 77 K. The luminescence spectra of **11**, **12**-OTf, and **13**-OTf almost coincide with the low-temperature spectra of the parent compound $Ir(ppy)_3$: in the cases of **12**-OTf and **13**-OTf, the coincidence is complete,[52a] while the emission is red-shifted by ca. 1100 cm^{-1} in **11**, which features the ruthenium OM-linker **2**. The registered lifetimes are all on the order of 5 μs, and this leads to the conclusion that the low-temperature emission registered for **11**−**13** is the typical mixed ^{3}LC−^{3}MLCT emission originating from the Ir^{III}ppy moiety.[52a,58] The

dx.doi.org/10.1021/ic202021w | Inorg. Chem. 2012, 51, 1739−1750

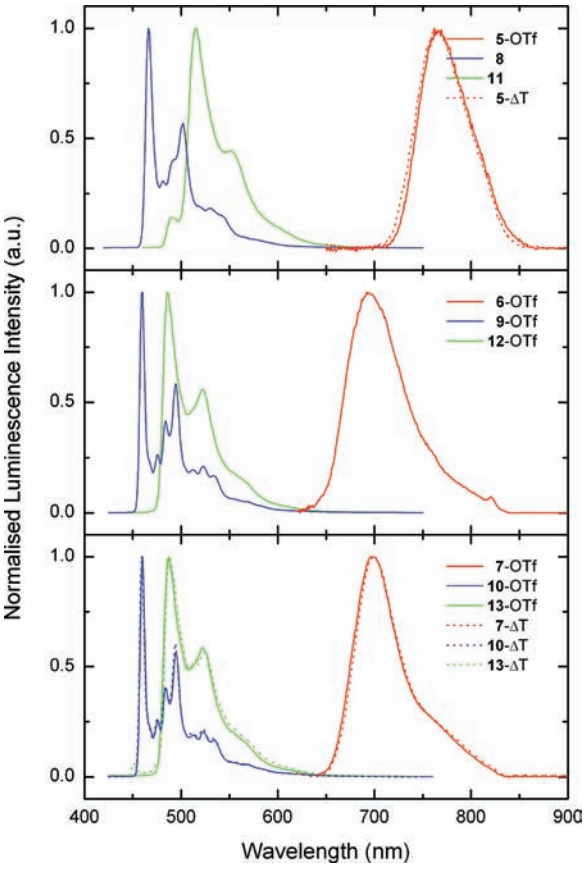

Figure 6. Emission spectra of bimetallic complexes **5**−**13** in a MeOH/EtOH glassy frozen solution at 77 K.

rhodium(III) derivatives **8**, **9**-OTf, and **10**-OTf exhibit a very intense and well-structured emission (Figure 6), typical of the rhodium cyclometalated derivatives,[52b] with lifetimes of around 95 μs (Table 2). The same structured and long-lived emission has been reported for the parent $[Rh(ppy)_2(bpy)]^+$ at 77 K and has been attributed to ppy-based LC phosphorescence, induced by the high spin−orbit coupling constant of rhodium.[52b] Even in this series the emission intensity maximum of **8** with the anionic ruthenium OM-linker **2** is slightly shifted to lower energies, but to a lesser extent (ca. 300 cm^{-1}) with respect to the related iridium(III) series. Thus, OM-linker **2** has a stronger effect on the excited-state properties of the $Ir(ppy)_2$ moieties than on the $Rh(ppy)_2$ moieties. Remarkably, we have found that ruthenium(II) derivatives **5**-OTf, **6**-OTf, and **7**-OTf in a frozen solvent show NIR phosphorescence with luminescence spectra that are strongly red-shifted and less structured compared to the spectrum of the reference $Ru(bpy)_3Cl_2$ measured in the same conditions.[55] The observed lifetimes (on the order of 1.2 μs) are lower than those obtained for $Ru(bpy)_3Cl_2$ (4.1 μs), as predicted by the energy gap law.[59] In this series of complexes, the ^{3}MLCT emission of the ruthenium(II) polypyridine fragment is strongly influenced by the presence of the OM unit. It is noteworthy that NIR phosphorescence is of prime importance for the development of optical devices for biological applications, whereby such compounds are capable of emitting with microsecond lifetimes beyond 700 nm.[60]

All in all, we found that our OM-linkers **2**−**4** show strong electron-donating ability compared to common polypyridines such as bipyridine and phenanthroline and thus might destabilize the HOMOs and provoke the observed red shift in the emission. In particular, the anionic OM-linker **2** is the most efficient donor ligand, as observed in the luminescent properties of the above compounds. As a general observation, the examined binuclear complexes show, at low temperature, luminescence of the respective metal-bpy or -ppy moiety, with an influence of the attached OM-linker, which depends on the transition metal either in the octahedral environment or in the OM-linker.

Transient Absorption. In order to gain a more detailed description of the nature of the lowest triplet states involved in the photophysics of the examined compounds, which turned out to be nonemissive at room temperature, transient-absorption experiments upon excitation with a 18 ns pulse at 355 nm have been performed for all of the bi- and monometallic complexes of the series. Transient-absorption spectra have been observed only in two cases: the two $Rh(ppy)_2$ derivatives **9**-OTf and **10**-OTf. Their end-of-pulse spectra are shown in Figure 7, together with the decay kinetics

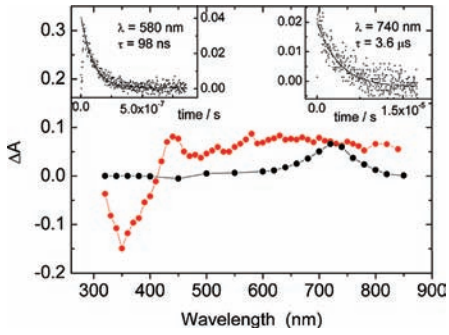

Figure 7. End-of-pulse transient-absorption spectra of **9**-OTf (black dots) and **10**-OTf (red dots) in an air-purged CH_2Cl_2 solution. Excitation at 355 nm, 4 mJ/pulse, A_{355} = 0.86. Left inset: ΔA decay at 580 nm for **10**-OTf. Right inset: ΔA decay at 740 nm for **9**-OTf.

derived at selected wavelengths. The spectrum of **10**-OTf shows ground-state depopulation features between 310 and 400 nm, a positive band at 440 nm, and a significant absorption that extends until 900 nm, with a lifetime of the transient species, equally derived at any wavelengths, of 98 ns. The spectral features closely resemble those reported for the lowest triplet of rhodium(III) polypyridine complexes,[52b,61] and also the lifetime is in the same range but somewhat reduced [τ = 250 ns for $Rh(phen)_3^{3+}$ in aqueous solutions].[62] The observed spectrum can thus be ascribed to absorption of the lowest triplet, mainly of LC nature, of the rhodium polypyridyl moiety, slightly affected by the presence of the iridium-containing OM-linker. In the case of **9**-OTf, the transient-absorption spectrum is rather different (Figure 7), with very low absorption until 650 nm, a clear and unique band centered at 740 nm, and a lifetime of 3.6 μs. To the best of our knowledge, there is only one reported case where a similar spectrum has been observed for $Rh_2(O_2CCH_3)_4(L)_2$ complexes (with L = CH_3OH, THF, or PPh_3).[63] In that case, the observed transient species showed a peak centered around 760 nm, invariant to the nature of the axial ligand L, with a lifetime in the range of 3.5−5.0 μs, and was tentatively attributed to an excited state involving π^* orbitals of the metal and carboxylate. It can thus be deduced that in **9**-OTf the presence of the OM-linker is strongly affecting the nature of the lowest triplet state observable at room temperature, leading to transitions that involve the

dx.doi.org/10.1021/ic202021w | Inorg. Chem. 2012, 51, 1739−1750

benzoquinone orbitals. DFT calculations performed on the first triplet excited state of **9**-OTf and **10**-OTf showed that in the latter the LUMOs are mainly localized on the $Rh(ppy)_2$ moiety of the complex (see the Supporting Information). Conversely, in the case of **9**-OTf, a contribution from the benzenedione fragment of the OM-linker for the same virtual orbitals is evident. The lack of detection of the lowest triplet state of the other component of the $Rh(ppy)_2$ family, i.e., **8**, can be attributed to a shortening of its lifetime due to the presence of the ruthenium OM counterpart or competitive electron-transfer process. Detection of the transient-absorption spectra in the nanosecond to microsecond time range only for $Rh(ppy)_2$ derivatives can be in accordance with the reported behavior of the lowest triplet states of rhodium(III) polypyridine complexes,[52b] which are poorly emissive at room temperature but clearly identifiable by their transient-absorption features. In the other complexes of the series, **5**−**7** and **11**−**13**, the lowest triplet states are probably quenched by competitive processes that strongly reduce also their luminescence, with respect to the normal room temperature emission features of the $Ir(ppy)_3$ and $[Ru(bpy)_3]Cl_2$ parent compounds, and are not detectable by the employed transient-absorption spectroscopy.

CONCLUSIONS

In this paper, we reported the synthesis of a novel family of luminescent coordination assemblies of the general formula $[M(L)_2(OM\text{-}linker)][X]_n$ (n = 0, 1, 2) where M = Ru, L = bpy and M = Rh, Ir, L = ppy. In these binuclear compounds, the luminophore brick adopts a distorted octahedral geometry due to the two polypyridine ligands and to cis O^O coordination of the OM-linkers $[Cp^*M(o\text{-}C_6H_4O_2)]^n$ [M = Ru, n = 1− (**2**); Rh, Ir, n = 0 (**3** and **4**)], as shown by the three X-ray molecular structures of **5**-OTf, **8**, and **11**. These OM-linkers are based on *o*-benzoquinone π-coordinated to Cp*M moieties (M = Ru, Rh, Ir). The UV−visible spectra of these binuclear complexes showed remarkable absorption bands that extend through the whole range of the visible spectrum and tail into the NIR region, especially in the case of the binuclear ruthenium derivative **5**-OTf, which confers to our complexes a panchromatic character. The emission properties recorded at low temperature show a red-shifted emission compared to those of the parent $[M(L\text{-}L)_3]$ (M = Ru, Rh, Ir) compounds with polypyridine or phenylpyridine ligands. Remarkably, in frozen media, the binuclear octahedral species **5**−**7** exhibited NIR phosphorescence. Our OM-linkers **2**−**4** exhibit strong donating ability compared to the common polypyridines such as bipyridine and phenanthroline and thus would destabilize the HOMOs and provoke the observed red shift. Remarkably, our complexes display clear luminescent features, in contrast to that reported for coordination compounds with a nonmetalated *o*-quinone ligand. The latter are nonluminescent because of the *o*-quinone ligand, which acts as a luminescence quencher. These important results pave the way for the preparation of new luminescent materials based on metalated quinonoid ligands for future applications in optoelectronic, photovoltaic, and sensing areas.

ASSOCIATED CONTENT

Supporting Information

Crystallographic data in CIF format for **5**, **8**, and **11** and additional computational data. This material is available free of charge via the Internet at http://pubs.acs.org.

AUTHOR INFORMATION

Corresponding Author

*E-mail: hani.amouri@upmc.fr (H.A.), andrea.barbieri@isof.cnr.it (A.B.).

ACKNOWLEDGMENTS

We thank CNRS, UPMC, French ANR (Project OPTO-ELECTR-OM ANR-11-BS07-001-01), and Italian CNR (Projects PM.P04.010 MACOL and ESF-EUROCORES Solar-FuelTandem) for supporting this work. H.A. thanks CNRS for providing a visiting fellowship grant to A.B. H.A. also thanks Dr. M. Rosa Axet for technical assistance and helpful discussions.

REFERENCES

(1) Hendrickson, D. N.; Pierpont, C. G. *Top. Curr. Chem.* **2004**, *234*, 63−95.
(2) Lever, A. B. P. *Coord. Chem. Rev.* **2010**, *254*, 1397−1405.
(3) Ward, M. D.; McCleverty, J. A. *J. Chem. Soc., Dalton Trans.* **2002**, 275−288.
(4) (a) Kaim, W.; Sarkar, B. *Coord. Chem. Rev.* **2007**, *251*, 584−594. (b) Boyer, J. L.; Rochford, J.; Tsai, M. K.; Muckerman, J. T.; Fujita, E. *Coord. Chem. Rev.* **2010**, *254*, 309−330.
(5) (a) da Silva, R. S.; Gorelsky, S. I.; Dodsworth, E. S.; Tfouni, E.; Lever, A. B. P. *J. Chem. Soc., Dalton Trans.* **2000**, 4078−4088. (b) Masui, H.; Freda, A. L.; Zerner, M. C.; Lever, A. B. P. *Inorg. Chem.* **2000**, *39*, 141−152.
(6) Mortimer, R. J. *Chem. Soc. Rev.* **1997**, *26*, 147−156.
(7) Hartl, F.; Rosa, P.; Ricard, L.; Le Floch, P.; Zalis, S. *Coord. Chem. Rev.* **2007**, *251*, 557−576.
(8) Nazeeruddin, M. K.; Pechy, P.; Renouard, T.; Zakeeruddin, S. M.; Humphry-Baker, R.; Comte, P.; Liska, P.; Cevey, L.; Costa, E.; Shklover, V.; Spiccia, L.; Deacon, G. B.; Bignozzi, C. A.; Gratzel, M. *J. Am. Chem. Soc.* **2001**, *123*, 1613−1624.
(9) Rice, C. R.; Ward, M. D.; Nazeeruddin, M. K.; Gratzel, M. *New J. Chem.* **2000**, *24*, 651−652.
(10) Marczak, R.; Werner, F.; Gnichwitz, J. F.; Hirsch, A.; Guldi, D. M.; Peukert, W. *J. Phys. Chem. C* **2009**, *113*, 4669−4678.
(11) Grange, C. S.; Meijer, A.; Ward, M. D. *Dalton Trans.* **2010**, *39*, 200−211.
(12) Spikes, G. H.; Bill, E.; Weyhermuller, T.; Wieghardt, K. *Angew. Chem., Int. Ed.* **2008**, *47*, 2973−2977.
(13) Lever, A. B. P.; Masui, H.; Metcalfe, R. A.; Stufkens, D. J.; Dodsworth, E. S.; Auburn, P. R. *Coord. Chem. Rev.* **1993**, *125*, 317−331.
(14) (a) Bhattacharya, S.; Pierpont, C. G. *Inorg. Chem.* **1992**, *31*, 35−39. (b) Bhattacharya, S.; Boone, S. R.; Fox, G. A.; Pierpont, C. G. *J. Am. Chem. Soc.* **1990**, *112*, 1088−1096.
(15) Wheeler, D. E.; McCusker, J. K. *Inorg. Chem.* **1998**, *37*, 2296−2307.
(16) Abuabara, S. G.; Cady, C. W.; Baxter, J. B.; Schmuttenmaer, C. A.; Crabtree, R. H.; Brudvig, G. W.; Batista, V. S. *J. Phys. Chem. C* **2007**, *111*, 11982−11990.
(17) (a) Hartl, F.; Vlcek, A. *Inorg. Chem.* **1996**, *35*, 1257−1265. (b) Hartl, F.; Vlcek, A. *Inorg. Chem.* **1992**, *31*, 2869−2876.
(18) (a) Moussa, J.; Rager, M. N.; Chamoreau, L. M.; Ricard, L.; Amouri, H. *Organometallics* **2009**, *28*, 397−404. (b) Lange, C. W.; Foldeaki, M.; Nevodchikov, V. I.; Cherkasov, V. K.; Abakumov, G. A.; Pierpont, C. G. *J. Am. Chem. Soc.* **1992**, *114*, 4220−4222.
(19) (a) Hirani, B.; Li, J.; Djurovich, P. I.; Yousufuddin, M.; Oxgaard, J.; Persson, P.; Wilson, S. R.; Bau, R.; Goddard, W. A.; Thompson, M. E. *Inorg. Chem.* **2007**, *46*, 3865−3875. (b) Barbaro, P.; Bianchini, C.; Frediani, P.; Meli, A.; Vizza, F. *Inorg. Chem.* **1992**, *31*, 1523−1529.
(20) Best, J.; Sazanovich, I. V.; Adams, H.; Bennett, R. D.; Davies, E. S.; Meijer, A.; Towrie, M.; Tikhomirov, S. A.; Bouganov, O. V.; Ward, M. D.; Weinstein, J. A. *Inorg. Chem.* **2010**, *49*, 10041−10056.

(21) (a) Le Bras, J.; Amouri, H.; Vaissermann, J. *J. Organomet. Chem.* **1998**, *553*, 483−485. (b) LeBras, J.; Rager, M. N.; Besace, Y.; Amouri, H.; Vaissermann, J. *Organometallics* **1997**, *16*, 1765−1771. (c) Moussa, J.; Guyard-Duhayon, C.; Herson, P.; Amouri, H.; Rager, M. N.; Jutand, A. *Organometallics* **2004**, *23*, 6231−6238.
(22) (a) Moussa, J.; Lev, D. A.; Boubekeur, K.; Rager, M. N.; Amouri, H. *Angew. Chem., Int. Ed.* **2006**, *45*, 3854−3858. (b) Moussa, J.; Rager, M. N.; Boubekeur, K.; Amouri, H. *Eur. J. Inorg. Chem.* **2007**, 2648−2653.
(23) Amouri, H.; Moussa, J.; Renfrew, A. K.; Dyson, P. J.; Rager, M. N.; Chamoreau, L. M. *Angew. Chem., Int. Ed.* **2010**, *49*, 7530−7533.
(24) Moussa, J.; Amouri, H. *Angew. Chem., Int. Ed.* **2008**, *47*, 1372−1380.
(25) Moussa, J.; Wong, K. M. C.; Chamoreau, L. M.; Amouri, H.; Yam, V. W. W. *Dalton Trans.* **2007**, 3526−3530.
(26) Damas, A.; Ventura, B.; Axet, M. R.; Degli Esposti, A.; Chamoreau, L.-M.; Barbieri, A.; Amouri, H. *Inorg. Chem.* **2010**, *49*, 10762−10764.
(27) (a) Dembek, A. A.; Fagan, P. J. *Organometallics* **1995**, *14*, 3741−3745. (b) O'Connor, J. M.; Friese, S. J.; Rodgers, B. L.; Rheingold, A. L.; Zakharov, L. *J. Am. Chem. Soc.* **2005**, *127*, 9346−9347.
(28) Duisenberg, A. J. M.; Kroon-Batenburg, L. M. J.; Schreurs, A. M. M. *J. Appl. Crystallogr.* **2003**, *36*, 220−229.
(29) Blessing, R. H. *Acta Crystallogr., Sect. A* **1995**, *51*, 33−38.
(30) Altomare, A.; Cascarano, G.; Giacovazzo, C.; Guagliardi, A.; Burla, M. C.; Polidori, G.; Camalli, M. *J. Appl. Crystallogr.* **1994**, *27*, 435−436.
(31) Palatinus, L.; Chapuis, G. *J. Appl. Crystallogr.* **2007**, *40*, 786−790.
(32) Ventura, B.; Degli Esposti, A.; Koszarna, B.; Gryko, D. T.; Flamigni, L. *New J. Chem.* **2005**, *29*, 1559−1566.
(33) Frisch, M. J.; Trucks, G. W.; Schlegel, H. B.; Scuseria, G. E.; Robb, M. A.; Cheeseman, J. R.; Scalmani, G.; Barone, V.; Mennucci, B.; Petersson, G. A.; Nakatsuji, H.; Caricato, M.; Li, X.; Hratchian, H. P.; Izmaylov, A. F.; Bloino, J.; Zheng, G.; Sonnenberg, J. L.; Hada, M.; Ehara, M.; Toyota, K.; Fukuda, R.; Hasegawa, J.; Ishida, M.; Nakajima, T.; Honda, Y.; Kitao, O.; Nakai, H.; Vreven, T.; Montgomery, J. A. J.; Peralta, J. E.; Ogliaro, F.; Bearpark, M.; Heyd, J. J.; Brothers, E.; Kudin, K. N.; Staroverov, V. N.; Kobayashi, R.; Normand, J.; Raghavachari, K.; Rendell, A.; Burant, J. C.; Iyengar, S. S.; Tomasi, J.; Cossi, M.; Rega, N.; Millam, N. J.; Klene, M.; Knox, J. E.; Cross, J. B.; Bakken, V.; Adamo, C.; Jaramillo, J.; Gomperts, R.; Stratmann, R. E.; Yazyev, O.; Austin, A. J.; Cammi, R.; Pomelli, C.; Ochterski, J. W.; Martin, R. L.; Morokuma, K.; Zakrzewski, V. G.; Voth, G. A.; Salvador, P.; Dannenberg, J. J.; Dapprich, S.; Daniels, A. D.; Farkas, Ö.; Foresman, J. B.; Ortiz, J. V.; Cioslowski, J.; Fox, D. J. *GAUSSIAN 09*, revision A.1; Gaussian, Inc.: Wallingford, CT, 2009.
(34) (a) Hohenberg, P.; Kohn, W. *Phys. Rev.* **1964**, *136*, B864−B871. (b) Kohn, W.; Sham, L. J. *Phys. Rev.* **1965**, *140*, A1133−A1138.
(35) (a) Bauernschmitt, R.; Ahlrichs, R. *Chem. Phys. Lett.* **1996**, *256*, 454−464. (b) Casida, M. E.; Jamorski, C.; Casida, K. C.; Salahub, D. R. *J. Chem. Phys.* **1998**, *108*, 4439−4449. (c) Stratmann, R. E.; Scuseria, G. E.; Frisch, M. J. *J. Chem. Phys.* **1998**, *109*, 8218−8224.
(36) (a) Adamo, C.; Barone, V. *J. Chem. Phys.* **1999**, *110*, 6158−6170. (b) Adamo, C.; Scuseria, G. E.; Barone, V. *J. Chem. Phys.* **1999**, *111*, 2889−2899.
(37) Peterson, K. A.; Figgen, D.; Dolg, M.; Stoll, H. *J. Chem. Phys.* **2007**, *126*, 124101.
(38) Figgen, D.; Peterson, K. A.; Dolg, M.; Stoll, H. *J. Chem. Phys.* **2009**, *130*, 164108.
(39) (a) Hariharan, P. C.; Pople, J. A. *Theor. Chem. Acc.* **1973**, *28*, 213−222. (b) Hehre, W. J.; Ditchfield, R.; Pople, J. A. *J. Chem. Phys.* **1972**, *56*, 2257−2261.
(40) Zhao, Y.; Truhlar, D. G. *Theor. Chem. Acc.* **2008**, *120*, 215−241.
(41) Tomasi, J.; Mennucci, B.; Cammi, R. *Chem. Rev.* **2005**, *105*, 2999−3093.
(42) Schaftenaar, G.; Noordik, J. H. *J. Comput.-Aided Mol. Des.* **2000**, *14*, 123−134.
(43) Espinet, P.; Bailey, P. M.; Maitlis, P. M. *J. Chem. Soc., Dalton Trans.* **1979**, 1542−1547.
(44) Reingold, J. A.; Son, S. U.; Kim, S. B.; Dullaghan, C. A.; Oh, M.; Frake, P. C.; Carpenter, G. B.; Sweigart, D. A. *Dalton Trans.* **2006**, 2385−2398.
(45) (a) Vichard, D.; Gruselle, M.; Amouri, H.; Jaouen, G. *J. Chem. Soc., Chem. Commun.* **1991**, 46−48. (b) Vichard, D.; Gruselle, M.; Amouri, H.; Jaouen, G.; Vaissermann, J. *Organometallics* **1992**, *11*, 976−979.
(46) Damas, A.; Moussa, J.; Rager, M. N.; Amouri, H. *Chirality* **2010**, *22*, 889−895.
(47) (a) Favarger, F.; Goujon-Ginglinger, C.; Monchaud, D.; Lacour, J. *J. Org. Chem.* **2004**, *69*, 8521−8524. (b) Lacour, J.; Frantz, R. *Org. Biomol. Chem.* **2005**, *3*, 15−19. (c) Lacour, J.; Hebbe-Viton, V. *Chem. Soc. Rev.* **2003**, *32*, 373−382.
(48) Wu, C.; Chen, H. F.; Wong, K. T.; Thompson, M. E. *J. Am. Chem. Soc.* **2010**, *132*, 3133−3139.
(49) (a) Mimassi, L.; Cordier, C.; Guyard-Duhayon, C.; Mann, B. E.; Amouri, H. *Organometallics* **2007**, *26*, 860−864. (b) Mimassi, L.; Guyard-Duhayon, C.; Rager, M. N.; Amouri, H. *Inorg. Chem.* **2004**, *43*, 6644−6649.
(50) Amouri, H.; Caspar, R.; Gruselle, M.; Guyard-Duhayon, C.; Boubekeur, K.; Lev, D. A.; Collins, L. S. B.; Grotjahn, D. B. *Organometallics* **2004**, *23*, 4338−4341.
(51) Pierpont, C. G.; Buchanan, R. M. *Coord. Chem. Rev.* **1981**, *38*, 45−87.
(52) (a) Flamigni, L.; Barbieri, A.; Sabatini, C.; Ventura, B.; Barigelletti, F. *Top. Curr. Chem.* **2007**, *281*, 143−203. (b) Indelli, M. T.; Chiorboli, C.; Scandola, F. *Top. Curr. Chem.* **2007**, *280*, 215−255.
(53) Montalti, M.; Credi, A.; Prodi, L.; Gandolfi, M. T. *Handbook of Photochemistry*, 3rd ed.; CRC Press and Taylor & Francis: Boca Raton, FL, 2006.
(54) (a) Calogero, G.; Giuffrida, G.; Serroni, S.; Ricevuto, V.; Campagna, S. *Inorg. Chem.* **1995**, *34*, 541−545. (b) Polson, M.; Fracasso, S.; Bertolasi, V.; Ravaglia, M.; Scandola, F. *Inorg. Chem.* **2004**, *43*, 1950−1956.
(55) Campagna, S.; Puntoriero, F.; Nastasi, F.; Bergamini, G.; Balzani, V. *Top. Curr. Chem.* **2007**, *280*, 117−214.
(56) Cicogna, F.; Gaddi, B.; Ingrosso, G.; Marcaccio, M.; Marchetti, F.; Paolucci, D.; Paolucci, F.; Pinzino, C.; Viglione, R. *Inorg. Chim. Acta* **2004**, *357*, 2915−2932.
(57) (a) Tamayo, A. B.; Alleyne, B. D.; Djurovich, P. I.; Lamansky, S.; Tsyba, I.; Ho, N. N.; Bau, R.; Thompson, M. E. *J. Am. Chem. Soc.* **2003**, *125*, 7377−7387. (b) Wang, X. H.; Li, J. A.; Thompson, M. E.; Zink, J. I. *J. Phys. Chem. A* **2007**, *111*, 3256−3262.
(58) Collin, J. P.; Dixon, I. M.; Sauvage, J. P.; Williams, J. A. G.; Barigelletti, F.; Flamigni, L. *J. Am. Chem. Soc.* **1999**, *121*, 5009−5016.
(59) Meyer, T. J.; Caspar, J. V. *Chem. Rev.* **1985**, *85*, 187−218.
(60) Palmer, J. H.; Durrell, A. C.; Gross, Z.; Winkler, J. R.; Gray, H. B. *J. Am. Chem. Soc.* **2010**, *132*, 9230−9231.
(61) Turro, C.; Evenzahav, A.; Bossmann, S. H.; Barton, J. K.; Turro, N. J. *Inorg. Chim. Acta* **1996**, *243*, 101−108.
(62) Indelli, M. T.; Carioli, A.; Scandola, F. *J. Phys. Chem.* **1984**, *88*, 2685−2686.
(63) Bradley, P. M.; Bursten, B. E.; Turro, C. *Inorg. Chem.* **2001**, *40*, 1376−1379.